

See discussions, stats, and author profiles for this publication at: <https://www.researchgate.net/publication/260882143>

Interaction of Nucleobases and Aromatic Amino Acids with Graphene Oxide and Graphene Flakes

ARTICLE *in* JOURNAL OF PHYSICAL CHEMISTRY LETTERS · OCTOBER 2013

Impact Factor: 7.46 · DOI: 10.1021/jz401929h

CITATIONS

20

READS

77

3 AUTHORS:



[Hakkim Vovusha](#)

King Abdullah University of Science and Techn...

12 PUBLICATIONS 51 CITATIONS

[SEE PROFILE](#)



[Suparna Sanyal](#)

Uppsala University

46 PUBLICATIONS 748 CITATIONS

[SEE PROFILE](#)



[Biplab Sanyal](#)

Uppsala University

239 PUBLICATIONS 3,286 CITATIONS

[SEE PROFILE](#)

Interaction of Nucleobases and Aromatic Amino Acids with Graphene Oxide and Graphene Flakes

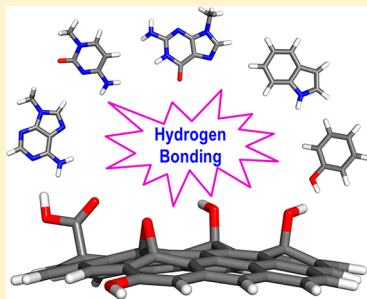
Hakkim Vovusha,^{†,‡} Suparna Sanyal,[‡] and Biplab Sanyal^{*,†}

[†]Department of Physics and Astronomy, Uppsala University, Box-516, 751 20 Uppsala, Sweden

[‡]Department of Cell and Molecular Biology, Uppsala University, Box-596, BMC, 751 24 Uppsala, Sweden

Supporting Information

ABSTRACT: In this work, we have studied interactions of nucleobases and aromatic amino acids with graphene (G) and graphene oxide (GO) flakes by ab initio density functional theory (DFT). It is evident from the results that GO complexes are stabilized by hydrogen bonding interactions whereas G complexes are stabilized by $\pi-\pi$ interactions, leading to enhanced binding energies for GO complexes compared to G complexes. Moreover, time-dependent DFT (TD-DFT) calculations for the optical properties reveal that the GO nanoflakes and GO–nucleobase composite absorb visible light in the range of 400–700 nm, which may be useful for light-emitting devices. The insights obtained from our study will be useful to understand the role of GO flakes as carriers in targeted drug delivery and biosensors.



SECTION: Molecular Structure, Quantum Chemistry, and General Theory

Since the discovery of graphene oxide (GO) in 2004,¹ different model structures of GO have been proposed^{2–5} based on several experimental and theoretical studies. GO is a graphene (G) sheet decorated with epoxide and hydroxyl groups on the basal plane as major components along with carbonyl and carboxyl groups on the edges as minor components. GO sheets consist of a hexagonal-ring-based carbon network having both sp^2 and sp^3 hybridized carbons.^{6–10} On the contrary, pristine G has sp^2 hybridized carbon atoms and hence has a flat surface. However, it has been shown by numerous studies that covalent functionalization of G sheets and edges of G nanoribbons can give rise to interesting electronic, magnetic, and transport properties.^{11–13}

GO has attracted great attention due to the water dispersity^{14,15} and amphiphilic^{16,17} character. It has many potential applications, such as biochemical sensing, cell imaging, and drug delivery, which are being investigated.^{18–20} Several applications of GO in biosystems have already been reported in the literature. It has been demonstrated that GO and GO composites possess antibacterial activity.²¹ The peptide toxins in drinking water can be removed by adsorption with a composite of smart RNA covalently immobilized with GO.²² Similarly, GO has been used to remove antibiotics from water.²³ Nuclease activity and cytotoxicity of small DNA intercalators are enhanced in the presence of GO.²⁴ It has been shown that GO interacts with DNA intercalators by noncovalent interactions to make new complex intercalators. Moreover, nanosized GO sheets with planar aromatic cyclic structures can act as potential DNA intercalators.

Recently, it has been demonstrated that nanomaterials with different functional groups on the surface can be used to bind the drug molecules with high affinity.^{25,26} Because GO has different functional groups present on its surface, it can be a

potential candidate as a drug carrier. It should be mentioned that planar carbon structures such as graphene and carbon nanotubes have already been tested as drug delivery carriers.²⁷ Thus, a comparative study of GO with these systems is highly relevant for different applications. The first step of designing a drug delivery vehicle is to study how it interacts with common biological molecules such as nucleic acids, proteins, or amino acids. These studies are highly important as one can get an idea of whether the carrier substance would affect the biological systems directly or indirectly.

Interactions of amino acids, DNA/RNA bases, and small molecules with G and carbon nanotubes are well studied using experimental and theoretical techniques.^{28–35} These studies indicate that noncovalent interactions such as $\pi-\pi$ stacking and X– π (X = CH, OH, NH, etc.) stabilize the nucleobase and amino acid complexes of G. In contrast, it has been suggested that GO interacts with proteins, nucleobases, and small molecules through noncovalent interactions.^{28–35} In addition to that, the interaction of GO with dye can be used as an optical sensor for DNA, which elicits the importance of optical techniques for study of interactions of biomolecules with nanomaterials.^{36,37} However, the understanding of the GO interactions at the molecular level is far from being complete as the fundamental knowledge of the nature of interactions between GO and these biomolecules is lacking. These studies are however highly significant as these will help to understand whether GO can be used as a suitable drug carrier or not.

Received: September 8, 2013

Accepted: October 16, 2013

Published: October 16, 2013

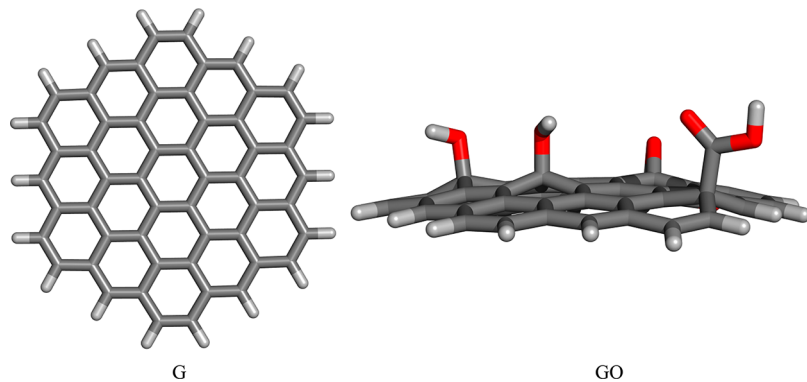


Figure 1. Optimized geometries of G and GO calculated with M05-2X.

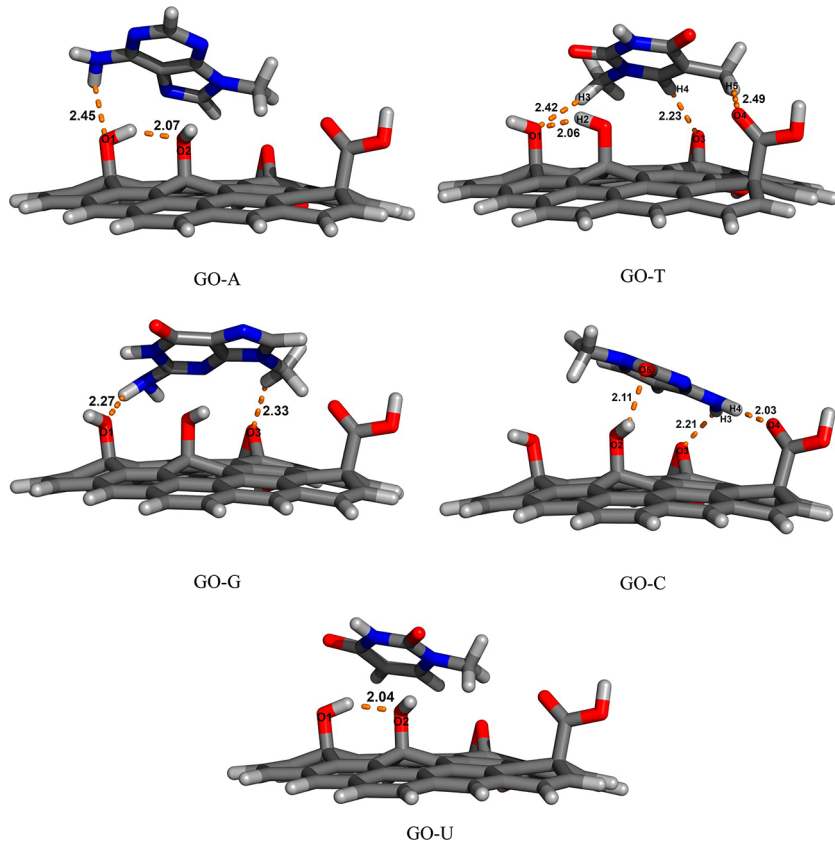


Figure 2. Optimized geometries (bond lengths in Å) of GO with DNA/RNA bases by M05-2X/6-31G(d).

To the best of our knowledge, theoretical studies on the interaction of GO with protein, DNA/RNA, and small molecules have not been reported. In this context, the objectives of the present investigation are to study (1) the energetics of GO with DNA/RNA bases adenine (A), guanine (G), cytosine (C), thymine (T) and uracil (U), and aromatic amino acids histidine (His), phenylalanine (Phe), tryptophan (Trp), and tyrosine (Tyr); (2) the nature of interaction of GO with DNA/RNA bases and aromatic amino acids; (3) the difference of similar interactions with G; (4) the structure and energetics of monohydroxyl (OH), monoepoxy (EPO), or monocarboxyl (CAR) of GO with DNA bases and aromatic amino acids; and (5) the optical properties of GO and graphene nanoflake (GNF).

In order to simulate G and GO, we have considered the GNF and graphene oxide nanoflake (GONF) as working models. We

are aware of the fact that due to the presence of finite size and edges, the properties estimated with these models may vary from those of the real systems to some extent. However, we expect that the results obtained with GNF and GONF will fit the bigger systems qualitatively, and thus, for simplification and convenience of calculations, use of the nanoflakes can be justified. The model structure of GONF used in this study is taken from the literature.³⁸ It has three hydroxyl and one epoxide groups on the basal plane and one carboxyl group on the edge. The initial geometry optimizations were carried out using the M05-2X functional with the 6-31G(d) basis set. Truhlar and co-workers have shown that M05-2X is suitable for studying noncovalent interactions.³⁹ The binding energies (BEs) of various complexes were calculated using M05-2X and M06-2X³⁹ with 6-31+G(d,p) and 6311++G(d,p) basis sets through the following equation:

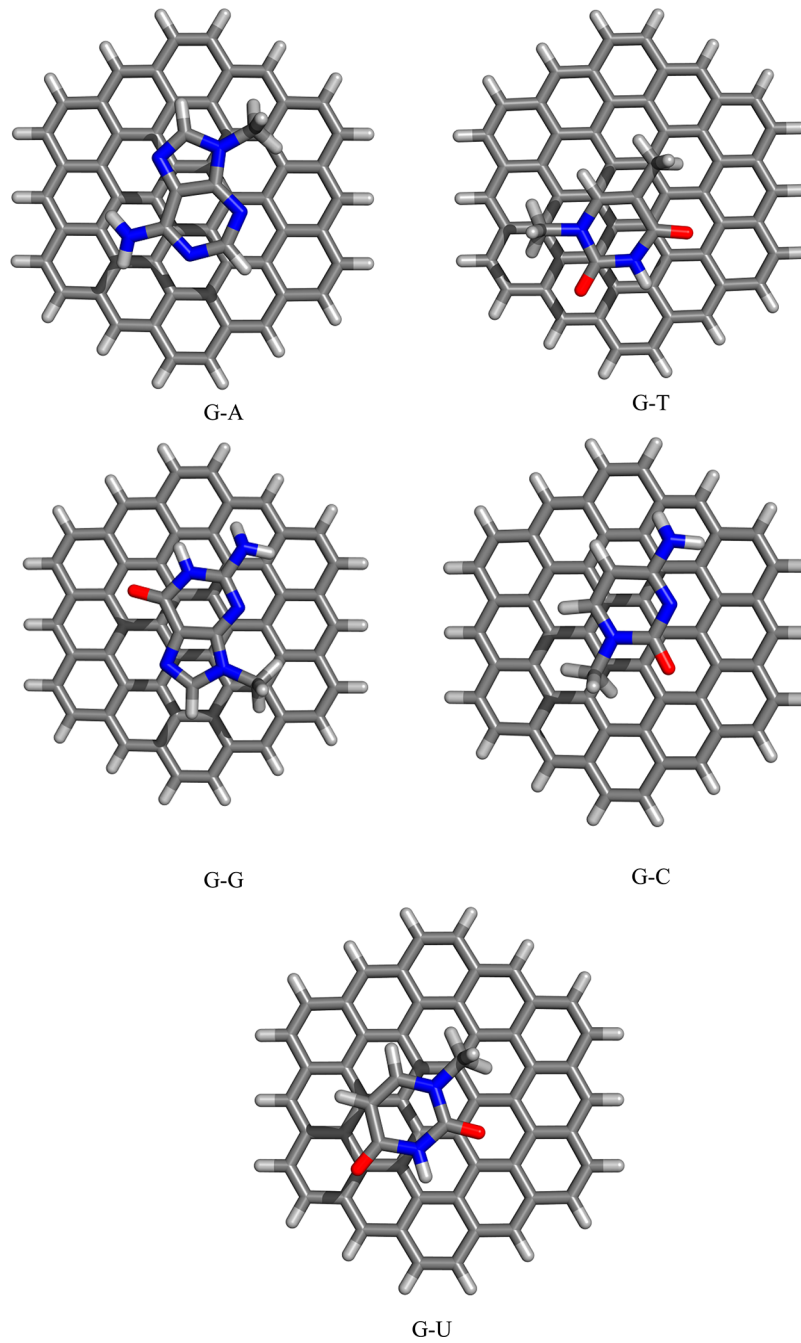


Figure 3. Optimized geometries of G with DNA/RNA bases by M05-2X/6-31G(d).

Table 1. Binding Energies (in kJ/mol) of GO and G with DNA/RNA Bases at the M05-2X Level of Theory^a

system	binding energy (kJ/mol)			
	G		GO	
	BE1	BE2	BE1	BE2
A	42.45	27.01	45.34	35.70
G	54.99	37.62	65.61	52.10
T	42.45	27.98	43.41	33.77
C	42.45	27.98	70.43	58.85
U	34.73	22.19	48.24	37.62

^aBE1: Binding energy without BSSE correction; BE2: binding energy with BSSE correction.

$$|BE| = (E_{\text{complex}} - \{(E_{\text{GO/G}}) + (E_{\text{AA/BP}})\})$$

The interaction energies were corrected with basis set superposition error (BSSE). Optical properties of GNF, GONF, and one of the complexes of GONF were calculated using the TD-M05-2X/6-31G(d) level of theory from the optimized geometries. All calculations have been performed using the Gaussian 09 package.⁴⁰

Optimized geometries of GNF and GONF are presented in Figure 1. From the figure, it is evident that the GONF has a buckled structure whereas GNF is planar. The buckling in GONF occurs due to the functional groups such as epoxy, hydroxyl, and carboxyl.

Optimized geometries of GO with DNA/RNA base are presented in Figure 2 along with important geometrical

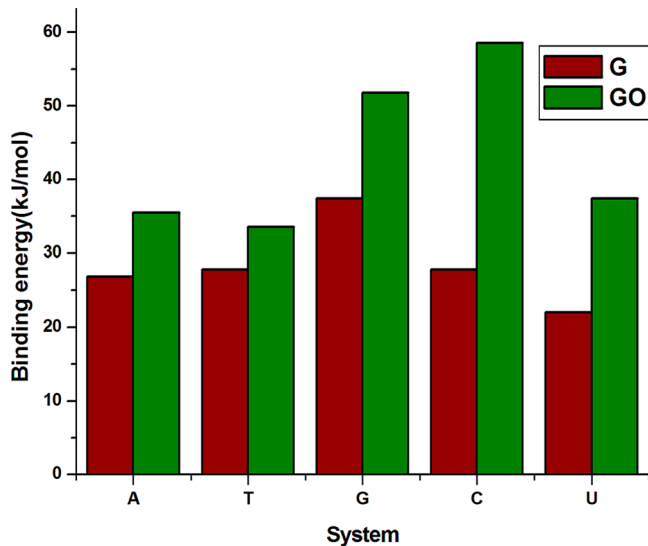


Figure 4. Comparison of binding energies of GO and G with DNA/RNA bases calculated by M05-2X/6-31+G(d,p).

parameters. In these complexes, nucleobases have van der Waals contact and/or hydrogen bond interactions with functional groups of GO. It is clearly visible that the bases are not oriented entirely parallel to the GO surface. It can be seen in Figure 3 that in GO–A, hydrogen bonding is observed between the two hydroxyl groups ($O_1\cdots H\cdots O_2$ is 2.07 \AA) of GO and the amine group of adenine along with one of the hydroxyl groups of GO ($O_1\cdots H$ is 2.45 \AA). In the case of GO–G, only the intermolecular hydrogen bond is observed, that is, $O_1\cdots H_2$ is 2.27 \AA and $O_3\cdots H$ is 2.33 \AA . In GO–T, both intra- and intermolecular hydrogen bonds are observed, that is, $O_1\cdots H_2$ is 2.06 \AA , $O_1\cdots H_3$ is 2.42 , $O_3\cdots H_4$ is 2.23 \AA , and $O_4\cdots H_5$ is 2.49 \AA . Similarly, for GO–C and GO–U, inter- and intramolecular hydrogen bondings are observed, respectively. For GO–C, the observed hydrogen bonds are $O_2\cdots H\cdots O_5$ at 2.11 \AA , $O_3\cdots H_3$ at 2.21 \AA , and $O_4\cdots H_3$ at 2.03 \AA , and for GO–U, the bond is $O_1\cdots H\cdots O_2$ at 2.04 \AA . To compare these structural and geometrical aspects with GNFs, the same types of calculations have been carried out for a GNF of similar size.

Figure 3 shows the optimized geometries of G with DNA/RNA bases. It is seen from the optimized geometries that in contrast to GNFs, the bases are oriented parallel to the surface of the GNF, and the vertical distance between G and the base is around $3.2\text{--}3.5\text{ \AA}$, which is similar to that of previous reports by Gowtham et al. and Sastry et al., showing the existence of the $\pi\cdots\pi$ interaction.^{28,31} The calculated BE of GO and G with bases using M05-2X/6-31+G(d,p) are presented in Table 1 and also graphically depicted in Figure 4. The observed trend for the GO with bases is found to be C > G > U > A > T. The strength of BE varies on the basis of the strength of hydrogen bonds in the complexes. Among all complexes, the highest BE is observed for the GO–C due to the presence of more hydrogen bonds. Similarly for G, the trend of BE is G > T = C > A > U. Using the extended basis set (6-311++G(d,p)), the decreasing order of BE for GO is the same as a smaller basis set like 6-31+G(d,p), that is, C > G > U > A > T (see the Supporting Information), and for G, the decreasing order of BE is G > C > T > A > U. We have compared the calculated BE of G and GO with nucleobases with the M062X method with 6-31+G(d,p) and 6-311++G(d,p) basis sets (see Supporting Information Table S1). The decreasing order of BE for GO complexes with the two above-mentioned basis sets is C > G > U > A > T. For G complexes, the same trend is seen with 6-31+G(d,p) of G > T > A > C > U, and for 6-311++G(d,p), it is G > T > C > A > U. The calculated BE for the G–G complex using the M06-2X method shows good agreement with the previous reports. It is well-established from experiment and theory that G can be used to sequence DNA.^{28–35} Because DNA bases bind with different BEs to GO, our results suggest that similar to G, GO can also be used for DNA sequencing. To explore the interaction of GO with the biological system further, we have made an attempt to study GO with aromatic amino acids.

Figure 5 shows the optimized structures and geometrical parameters of complexes having GO with different aromatic amino acids, namely, Tyr, Trp, Phe, and His. Intermolecular hydrogen bonding is observed for all of the complexes except GO–Phe because it does not have any heteroatom other than carbon and hydrogen. In GO–Tyr, the hydroxyl group of phenol is hydrogen bonded with the hydroxyl group of GO

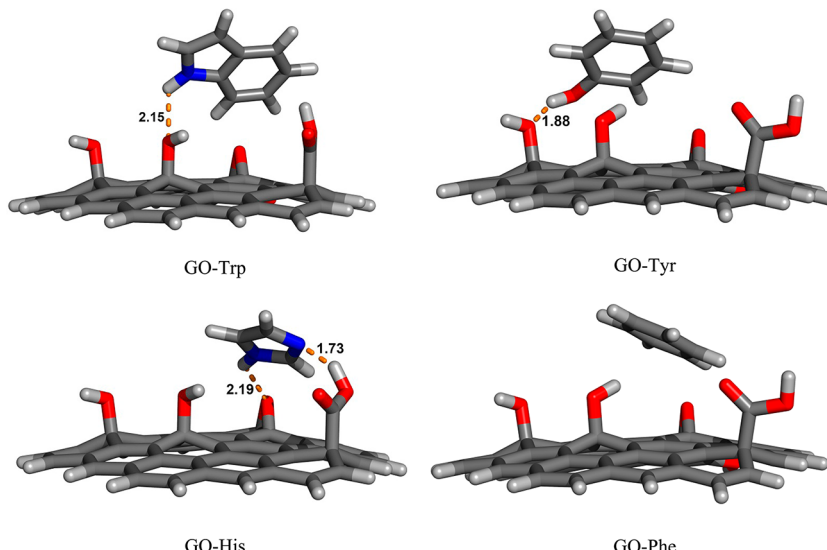


Figure 5. Optimized geometries (bond lengths in \AA) of GO with aromatic amino acids by M05-2X/6-31G(d).

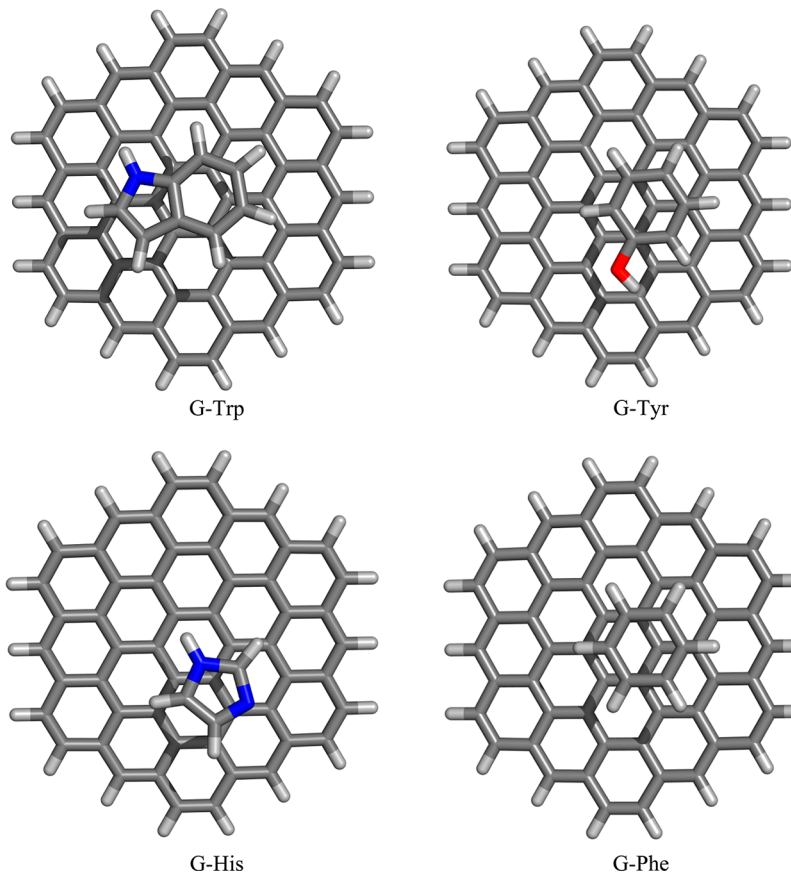


Figure 6. Optimized geometries of G with aromatic amino acids by M05-2X/6-31G(d).

Table 2. Binding Energies (in kJ/mol) of GO and G with Aromatic Amino Acids at the M05-2X Level of Theory^a

system	binding energy (kJ/mol)			
	G		GO	
	BE1	BE2	BE1	BE2
Tyr	27.84	16.32	48.00	38.40
Trp	36.48	24.00	50.88	43.20
Phe	23.04	14.40	26.88	20.16
His	23.04	14.40	95.04	86.40

^aBE1: Binding energy without BSSE correction; BE2: binding energy with BSSE correction.

(O1···H1 is 1.88 Å), whereas the hydroxyl group of GO is hydrogen bonded with indole ring hydrogen in the GO–Trp complex with a bond length of 2.15 Å. All of the atoms of the benzene ring have van der Waals contact with the GONF surface in the GO–Phe complex. In GO–His, the imidazole ring is doubly hydrogen bonded with the GONF surface, that is, O1···H1 is 2.19 Å and H2···N1 is 1.73 Å. Similar to the GONF with bases, calculations on the aromatic amino acids with GNF have been performed to have a comparison with the results of GONF. From Figure 6, it is realized that the aromatic amino acid rings are oriented parallel to the GNF, indicating the presence of π – π interaction. The vertical separations between the center of the GNF and aromatic rings are found to be 3.45, 3.21, 3.51, and 3.39 Å for Tyr, Trp, Phe, and His, respectively. These numbers are in very good agreement with those from the previous studies. The calculated BEs of GO and GNF with bases using M052X/6-31+G(d,p) are presented in

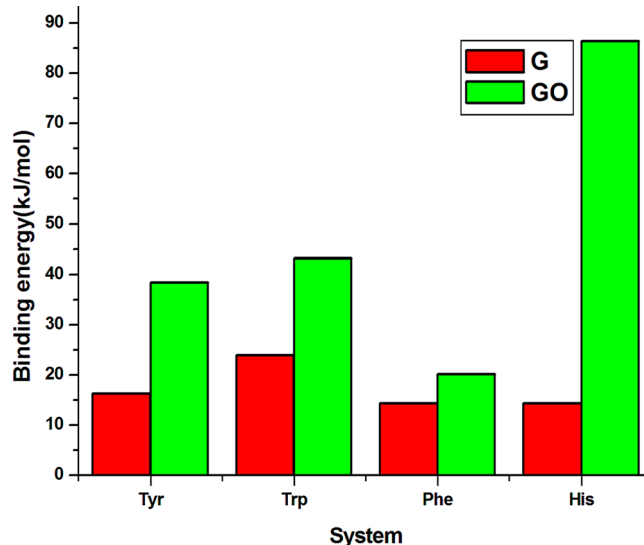


Figure 7. Comparison of binding energies of GO and G with aromatic amino acids by M05-2X/6-31+G(d,p).

Table 2. The BEs of all of the complexes are graphically depicted in Figure 7. The observed trend for the GONF with different aromatic amino acids is found to be His > Trp > Tyr > Phe, whereas the trend for GNF is Trp > Tyr > Phe = HIS. The highest BE for the GO–His is due to the presence of a double hydrogen bond. Like nucleobases, we have calculated the BEs of aromatic amino acids with GO and G with the extended basis set (6-311++G(d,p)), and the decreasing order of BE for

Table 3. Binding Energies (in kJ/mol) of Monohydroxyl, Epoxy, and Carboxy GO with Aromatic Amino Acids at the M05-2X Level of Theory^a

system	binding energy (kJ/mol)					
	OH		EPO		CAR	
	BE1	BE2	BE1	BE2	BE1	BE2
A	31.68	20.16	49.92	35.52	48.00	33.60
G	83.52	68.16	62.40	46.08	63.36	47.04
T	65.28	51.84	49.92	35.52	69.12	58.56
C	62.40	48.96	55.68	41.28	54.72	40.32
U	40.32	29.76	47.04	33.60	45.12	31.68
Tyr	44.16	33.60	27.84	17.28	32.64	21.12
Trp	32.64	24.00	36.48	25.92	43.20	34.56
Phe	23.04	15.36	25.92	17.28	28.80	20.16
His	45.12	36.48	37.44	28.80	54.72	59.52

^aBE1: Binding energy without BSSE correction; BE2: binding energy with BSSE correction.

GO is His > Trp > Tyr > Phe, similar to that of the 6-31+G(d,p) basis set (see Supporting Information Table S1), and for G, the decreasing order of the BE is Trp > Tyr > His > Phe. We have compared the calculated BE of G and GO with aromatic amino acids using the M062X method with the 6-31+G(d,p) and 6-311++G(d,p) basis sets (see the Supporting Information). The decreasing order of the BE for GO complexes with the two above-mentioned basis sets is His > Tyr > Trp > Phe. For G complexes, the trend is Trp > Tyr > Phe > His. Rajesh et al.²⁷ have performed detailed analysis of the interaction of aromatic amino acids with G and nanotubes, and the BE trend for both nanomaterials is Trp > Tyr > Phe > His, which is good agreement with the results obtained from the present studies.

To elucidate the role of an individual functional group of GO in dictating the BE of complexes, we have calculated the BE of GONF with a OH, EPO, or CAR group with DNA bases and aromatic amino acids with the M05-2X/6-31G(d)/6-311+G(d, p) level of calculation. The optimized geometry of the complexes is given in the Supporting Information (Figure S4). The calculated BEs of the complexes are listed in Table 3. The range of BEs for the GO with DNA bases is 43.41–70.43

kJ/mol and with OH, EPO, and CAR, the BE ranges are 31.84–83.94, 47.27–62.71, and 45.34–69.46 kJ/mol; with aromatic amino acids, the BE is 27.01–95.52, and with OH, EPO, and CAR, the BE ranges are 23.15–45.34, 26.05–37.62, and 28.94–54.99 kJ/mol. It is clear from the results that the BE with OH, EPO, and CAR is more or less similar to that for GONF complexes, and depending on the number and strength of hydrogen bonds, the BE of OH, EPO, and CAR varies. For example, OH–G has a higher BE than the EPO and CAR due to the presence of a double hydrogen bond, and the hydrogen bond distance is also shorter than the others (see Supporting Information Figure S4). Therefore, these findings elicit that all of the groups are contributing significantly to the BE of the complexes.

Caetano and co-workers have calculated UV-visible absorption spectra of different sizes of GNFs using TD-DFT calculations.⁴¹ The results show that GNFs yield a full range of the visible spectrum, which is a suitable criterion to produce light-emitting devices. Recently, Balapanaru et al. reported that functionalized GO can be used as an optical sensor for DNA detection, and they used UV-visible absorption and fluorescence spectroscopy to probe the complex of GO–dye and GO–dye–DNA.³⁶ In this context, we have also used the TD-DFT method to unravel the optical properties of GNF and GONF. In addition, we have predicted optical properties of one of the GONF complexes, namely, G–A and GO–A. Simulated absorption spectra of GO, G, G–A, and GO–A are depicted in Figure 8. To understand the nature of transition, the isosurface of orbitals involved in the transition has been plotted with a 0.02 au value, which is shown in Figures 9 and 10. The isodensity plots of the orbitals have π -type molecular orbital characteristics. We have observed three peaks at 250, 274, and 354 nm for GNF, which correspond to a $\pi-\pi^*$ transition of aromatic the $-C=C$ bond. The dominant absorption band (354 nm) is associated with an electronic transition from HOMO–1 to LUMO+1. The second (274 nm) and third (250 nm) bands are associated with H–1–L+7 and H–6–L transitions, respectively. As shown in Figure 8, the dominant band of G–A appears at 356 nm (H–1–L+1), and the second and third bands are observed at 274 (H–L+7) and 255 (H–2–L+3) nm, respectively. For GONF, we have observed two

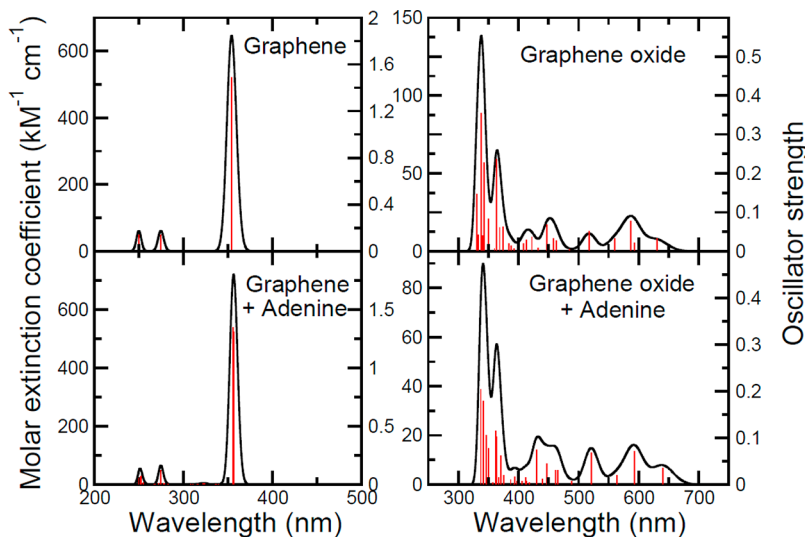


Figure 8. The absorption spectra of G, G–A, GO, and GO–A computed at the M05-2X/6-31+G(d,p) level of theory.

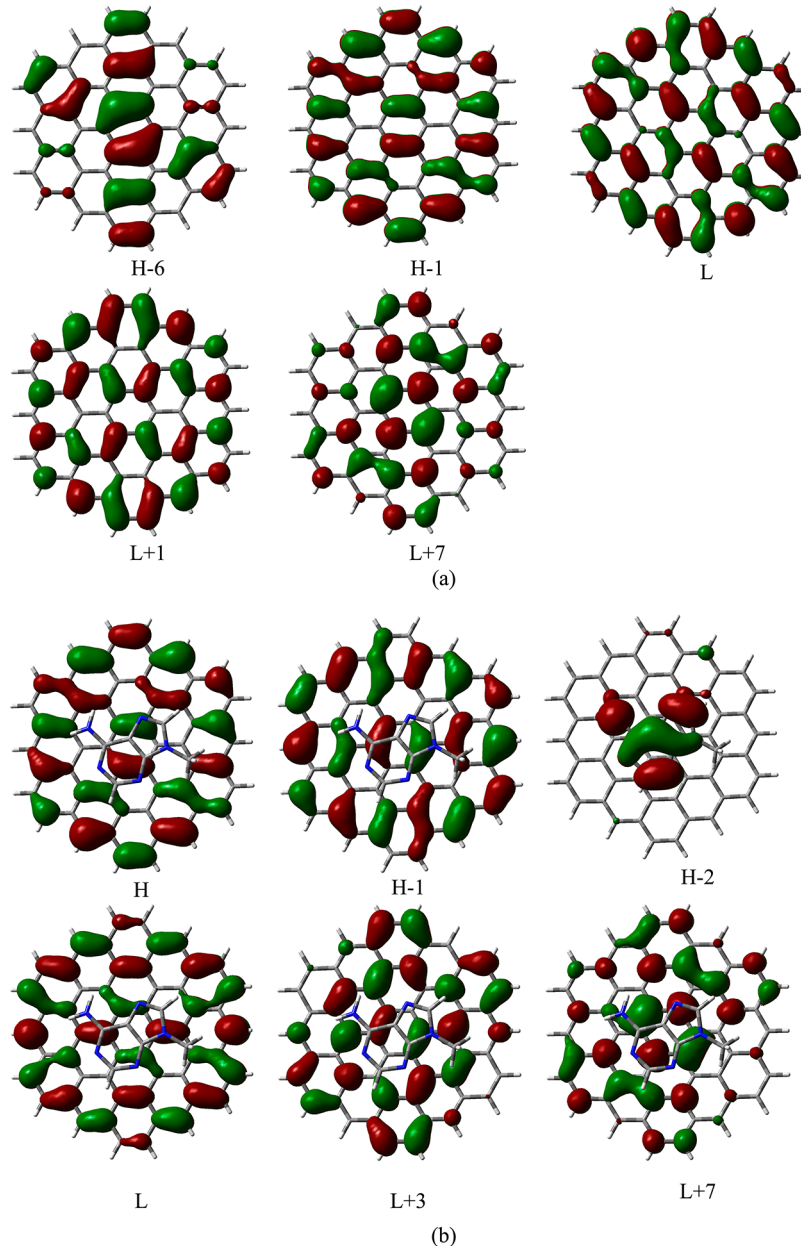


Figure 9. The isosurfaces of molecular orbitals of (a) G and (b) G-A calculated at the M05-2X/6-31+G(d,p) level of theory.

major absorption peaks at 341 (H-1-L+1) and 367 (H-3-L) nm, which correspond to $n-\pi^*$ of the C=O bond. The corresponding peaks for the GO-A complex were similar, at 337 and 362 nm, respectively. For both GONF and GO-A, additional small peaks were visible in the range of 380–650 nm (Figure 8). These peaks are absent in GNF due to the absence of the functional groups such as hydroxyl, epoxy, and carboxyl groups. Orbitals associated with these transitions are given in the Supporting Information (Figures S1, S2, and S3). Changes in the absorption wavelength of GO and GO-A are small (~ 5 nm). It is clear from the results that GONF absorbs in the full range of the visible spectrum (400–700 nm), which is a new finding. Therefore, one may conclude that similar to GNF, GONF can also be used to produce light-emitting devices. Nanoflake films are used as nanostructured electrodes for biomolecular sensing and energy storage/conversion applications.³⁵ Thus, it seems that similar to G and other nanoflakes, GONFs can also be used to sense the biomolecule.

In Table 4, we present the calculated values of HOMO–LUMO gaps of the bases and amino acids complexes with GONF and GNF. GONF complexes considered in this study are radical systems with α and β HOMO–LUMO gaps. The calculated α and β HOMO–LUMO gaps of GONF are 3.61 and 3.76 eV, respectively, whereas for the GNF, the value is 4.45 eV. The calculated α HOMO–LUMO gaps of GONF complexes vary in the order GO-C > GO-U = GO-A > GO-G > GO-T, and for β the trend is GO-T > GO-A = GO-U > GO-C > GO-G. Similarly, for the GNF complexes, the gaps vary as G-A > G-U > G-T > G-C > G-G. However, there is no noticeable change in the HOMO–LUMO gap value for complexes when compared to that of isolated flake.

The interaction of nucleobases and aromatic amino acids with GO and G nanoflakes was studied using DFT along with the optical properties of GO and G nanoflakes using TD-DFT.

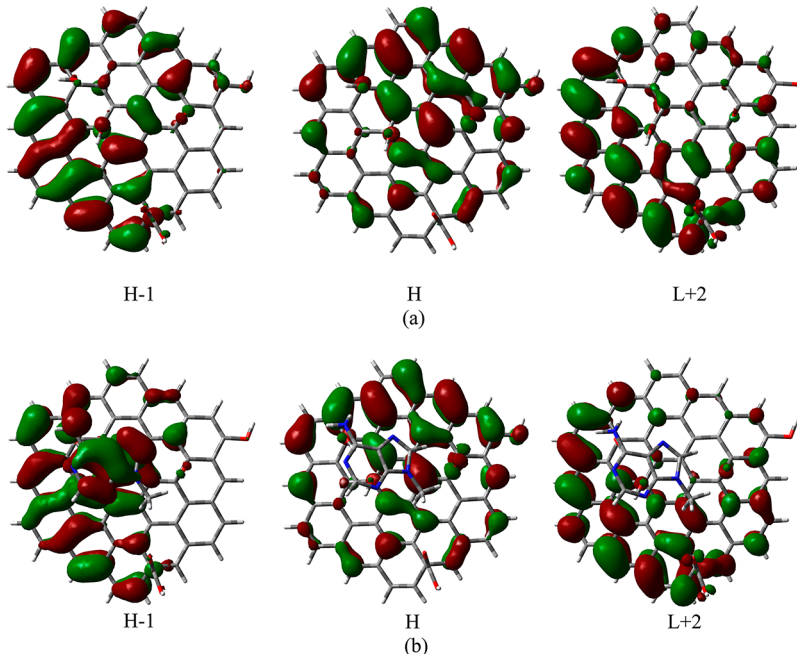


Figure 10. The isosurfaces of molecular orbitals of (a) GO and (b) GO-A calculated at the M05-2X/6-31+G(d,p) level of theory.

Table 4. HOMO–LUMO Gap (in eV) of GO and G with DNA/RNA Bases and Aromatic Amino Acids at the M05-2X/6-31G(d) Level of Theory

	HOMO–LUMO gap(eV)		
	G	GO	
		α	β
A	4.44	3.60	3.75
G	4.42	3.58	3.54
T	4.43	3.55	3.80
C	4.42	3.67	3.73
U	4.44	3.60	3.75
TYR	4.44	3.58	3.78
TRP	4.45	3.49	3.83
PHE	4.45	3.63	3.73
HIS	4.44	3.46	3.87
G	4.45		
GO	3.61(α)	3.76(β)	

On the basis of the structural models considered in this study, the significant observations are the following.

(i) Nucleobases and aromatic amino acids do not have parallel orientation with the GO surface as in the G surface. GO complexes are stabilized by hydrogen-bonding interactions between GO and bases or amino acids, whereas G complexes are stabilized by π - π interactions. The order of BEs between GO and nucleobases using M05-2X with 6-31+G(d,p) and 6-311++G(d,p) basis sets are C > G > U > A > T, and the trend for M06-2X is C > G > U > A > T. With G, the order is G > T = C > A, and with M06-2X, the order is G > T > A > C > U. For aromatic amino acids, the order of interaction of GO with M05-2X is His > Trp > Tyr > Phe, whereas for G, it is Trp > Tyr > Phe = His. Using M06-2X, the BE trend of the GO complex is His > Tyr > Trp > Phe, and for G, the trend is Trp > Tyr > Phe > His. In the case of OH, EPO, or CAR GO complexes, the range of calculated BEs is similar to that of GO complexes. The HOMO–LUMO gaps of GO and its complexes are smaller than those with G.

(ii) GONF absorbs at 337 nm, which corresponds to a n– π^* transition, and GNF absorbs at 274 nm, corresponding to the π – π^* transition, which is in good agreement with available experimental observation.^{36,41} GONF absorbs in the full range of visible light and therefore can be used to produce light-emitting devices. The results obtained from the present investigation are very useful to the understanding of GO with drug molecules and sensing of biomolecules with nanoflakes.

ASSOCIATED CONTENT

S Supporting Information

Calculated M06-2X method binding energies of GO and G with nucleobases and aromatic amino acids, vertical excitation process of G, GO, and the GO–A complex, and optimized geometries of monofunctional group GO with nucleobases and aromatic amino acids. This material is available free of charge via the Internet at <http://pubs.acs.org>.

AUTHOR INFORMATION

Corresponding Author

*E-mail: biplab.sanyal@physics.uu.se.

Notes

The authors declare no competing financial interest.

ACKNOWLEDGMENTS

This work is supported by the individual grants from the Swedish Research Council and Carl Tryggers Stiftelse (to S.S. and B.S.); VR-SIDA (Swedish Research Links) to B.S.; and Linnaeus grant (Uppsala RNA Research Center), Knut and Alice Wallenberg Foundation (RiboCORE) to S.S. We gratefully acknowledge supercomputing time allocation by the Swedish National Infrastructure for Computing (SNIC) for performing the computations.

■ REFERENCES

- (1) Novoselov, K. S.; Geim, A. K.; Morozov, S. V.; Jiang, D.; Zhang, Y.; Dubonos, S. V.; Grigorieva, I. V.; Firsov, A. Electric Field Effect in Atomically Thin Carbon Films. *A. Science* **2004**, *306*, 666–669.
- (2) Dreyer, D. R.; Park, S.; Bielawski, C. W.; Ruoff, R. S. The Chemistry of Graphene Oxide. *Chem. Soc. Rev.* **2010**, *39*, 228–240.
- (3) Lerf, A.; He, H. Y.; Forster, M.; Klinowski, J. Structure of Graphite Oxide Revisited. *J. Phys. Chem. B* **1998**, *102*, 4477–4482.
- (4) Ruoff, R. S. Calling All Chemists. *Nat. Nanotechnol.* **2008**, *3*, 10–11.
- (5) Gao, W.; Alemany, L. B.; Ci, L.; Ajayan, P. M. New Insights into the Structure and Reduction of Graphite Oxide. *Nat. Chem.* **2009**, *1*, 403–408.
- (6) Lui, C. H.; Liu, L.; Mak, K. F.; Flynn, G. W.; Heinz, T. F. Ultraflat Graphene. *Nature* **2009**, *462*, 339–341.
- (7) Szabo, T.; Berkesi, O.; Forgo, P.; Josepovits, K.; Sanakis, Y.; Petridis, D.; Dekany, I. Evolution of Surface Functional Groups in a Series of Progressively Oxidized Graphite Oxides. *Chem. Mater.* **2006**, *18*, 2740–2749.
- (8) Elias, D. C.; Nair, R. R.; Mohiuddin, T. M. G.; Morozov, S. V.; Blake, P.; Halsall, M. P.; Ferrari, A. C.; Boukhvalov, D. W.; Katsnelson, M. I.; Geim, A. K.; et al. Control of Graphene's Properties by Reversible Hydrogenation: Evidence for Graphane. *Science* **2009**, *323*, 610–613.
- (9) Eda, G.; Mattevi, C.; Yamaguchi, H.; Kim, H.; Chhowalla, M. Insulator to Semimetal Transition in Graphene Oxide. *J. Phys. Chem. C* **2009**, *113*, 15768–15771.
- (10) Gomez-Navarro, C.; Weitz, R. T.; Bittner, A. M.; Scolari, M.; Mews, A.; Burghard, M.; Kern, K. Electronic Transport Properties of Individual Chemically Reduced Graphene Oxide Sheets. *Nano Lett.* **2007**, *7*, 3499–3503.
- (11) Sanyal, B.; Eriksson, O.; Jansson, U.; Grennberg, H. Molecular Adsorption in Graphene with Divacancy Defects. *Phys. Rev. B* **2009**, *79*, 113409–113414.
- (12) Chandrachud, P.; Pujari, B. S.; Haldar, S.; Sanyal, B.; Kanhere, D. G. A Systematic Study of Electronic Structure from Graphene to Graphane. *J. Phys.: Condens. Matter* **2010**, *22*, 465502–465513.
- (13) Bhandary, S.; Eriksson, O.; Sanyal, B.; Katsnelson, M. I. Complex Edge Effects in Zigzag Graphene Nanoribbons Due to Hydrogen Loading. *Phys. Rev. B* **2010**, *82*, 165405–165412.
- (14) Li, D.; Kaner, R. B. Graphene-Based Material. *Science* **2008**, *320*, 1170–1171.
- (15) Dikin, D. A.; Stankovich, S.; Zimney, E. J.; Piner, R. D.; Dommett, G. H. B.; Evmenenko, G.; Nguyen, S. T.; Ruoff, R. S. Preparation and Characterization of Graphene Oxide Paper. *Nature* **2007**, *448*, 457–460.
- (16) Cote, L. J.; Kim, F.; Huang, J. X. Langmuir–Blodgett Assembly of Graphite Oxide Single Layers. *J. Am. Chem. Soc.* **2009**, *131*, 1043–1049.
- (17) Kim, J.; Cote, L. J.; Kim, F.; Yuan, W.; Shull, K. R.; Huang, J. X. Graphene Oxide Sheets at Interfaces. *J. Am. Chem. Soc.* **2010**, *132*, 8180–8186.
- (18) Chen, F. M.; Liu, S. B.; Shen, J. M.; Wei, L.; Liu, A. D.; Chan-Park, M. B.; Chen, Y. Ethanol-Assisted Graphene Oxide-Based Thin Film Formation at Pentane–Water Interface. *Langmuir* **2011**, *27*, 9174–9181.
- (19) Feng, L. Z.; Liu, Z. A. Graphene in Biomedicine: Opportunities and Challenges. *Nanomedicine* **2011**, *6*, 317–324.
- (20) Kuila, T.; Bose, S.; Khanra, P.; Mishra, A. K.; Kim, N. H.; Lee, J. H. Recent Advances in Graphene-Based Biosensors. *Biosens. Bioelectron.* **2011**, *26*, 4637–4648.
- (21) Liu, S.; Hu, M.; Zeng, T. H.; Wu, R.; Jiang, R.; Wei, J.; Wang, L.; Kong, J.; Chen, Y. Lateral Dimension Dependent Antibacterial Activity of Graphene Oxide Sheets. *Langmuir* **2012**, *28*, 12364–12372.
- (22) Hua, X.; Mub, L.; Wenb, J.; Zhoua, Q. Immobilized Smart RNA On Graphene Oxide Nanosheets to Specifically Recognize and Adsorb Trace Peptide Toxins in Drinking Water. *J. Hazard. Mater.* **2012**, *213–214*, 387–392.
- (23) Gao, Y.; Li, Y.; Zhang, L.; Huang, H.; Hu, J.; Shah, S. M.; Su, X. Adsorption and Removal of Tetracycline Antibiotics from Aqueous Solution by Graphene Oxide. *J. Colloid Interface Sci.* **2012**, *368*, 540–546.
- (24) Zheng, B.; Wang, C.; Wu, C.; Zhou, X.; Lin, M.; Wu, X.; Xin, X.; Chen, X.; Xu, L.; Liu, H.; et al. Nuclease Activity and Cytotoxicity Enhancement of the DNA Intercalators via Graphene Oxide. *J. Phys. Chem. C* **2012**, *116*, 15839–15846.
- (25) Chi, F. L.; Guo, Y. N.; Liu, J.; Liu, Y. L.; Huo, Q. S. Size-Tunable and Functional Core–Shell Structured Silica Nanoparticles for Drug Release. *J. Phys. Chem. C* **2010**, *114*, 2519–2523.
- (26) Ferrari, M. Cancer Nanotechnology: Opportunities and Challenges. *Nat. Rev. Cancer* **2005**, *5*, 161–171.
- (27) Rajesh, C.; Majumder, C.; Mizuseki, H.; Kawazoe, Y. A Theoretical Study on the Interaction of Aromatic Amino Acids with Graphene and Single Walled Carbon Nanotube. *J. Chem. Phys.* **2009**, *130*, 124911–124916.
- (28) Umadevi, D.; Sastry, G. N. Quantum Mechanical Study of Physisorption of Nucleobases on Carbon Materials: Graphene versus Carbon Nanotubes. *J. Phys. Chem. Lett.* **2011**, *2*, 1572–1576.
- (29) Chen, R. J.; Bangsaruntip, S.; Drouvalakis, K. A.; Kam, N. W. S.; Shim, M.; Li, Y.; Kim, W.; Utz, P. J.; Dai, H. Noncovalent Functionalization of Carbon Nanotubes for Highly Specific Electronic Biosensors. *Proc. Natl. Acad. Sci. U.S.A.* **2003**, *100*, 4984–4989.
- (30) Varghese, N.; Mogera, U.; Govindaraj, A.; Das, A.; Maiti, P. K.; Sood, A. K.; Rao, C. N. R. Binding of DNA Nucleobases and Nucleosides with Graphene. *ChemPhysChem* **2009**, *10*, 206–210.
- (31) Gowtham, S.; Scheicher, R. H.; Ahuja, R.; Pandey, R.; Karna, S. P. Physisorption of nucleobases on Graphene: Density-Functional Calculations. *Phys. Rev. B* **2007**, *76*, 033401–033405.
- (32) Cazorla, C. Ab Initio Study of the Binding of Collagen Amino Acids to Graphene and A-Doped (A = H, Ca) Graphene. *Thin Solid Films* **2010**, *518*, 6951–6961.
- (33) Kang, H. S. Theoretical Study of Binding of Metal-Doped Graphene Sheet and Carbon Nanotubes with Dioxin. *J. Am. Chem. Soc.* **2005**, *127*, 9839–9843.
- (34) Cazorla, C.; Rojas-Cervellera, V.; Rovira, C. Calcium-Based Functionalization of Carbon Nanostructures for Peptide Immobilization in Aqueous Media. *J. Mater. Chem.* **2012**, *22*, 19684–19693.
- (35) Roman, T.; Dinyo, W. A.; Nakanishi, H.; Kasai, H. Glycine Adsorption on Single-Walled Carbon Nanotubes. *Thin Solid Films* **2006**, *509*, 218–222.
- (36) Balapanuru, J.; Yang, J.; Xiao, S.; Bao, Q.; Jahan, M.; Polavarapu, L.; Wei, J.; Xu, Q. H.; Loh, K. P. A Graphene Oxide–Organic Dye Ionic Complex with DNA-Sensing and Optical-Limiting Properties. *Angew. Chem.* **2010**, *122*, 6699–6703.
- (37) Xing, X.-J.; Liu, X.-G.; He, Y.; Lin, Y.; Zhang, C.-L.; Tang, H.-W.; Pang, D.-W. Amplified Fluorescent Sensing of DNA Using Graphene Oxide and a Conjugated Cationic Polymer. *Biomacromolecules* **2013**, *14*, 117–123.
- (38) Rosas, J. J. H.; Gutiérrez, R. E. R.; Escobedo-Morales, A.; Anota, E. C. First Principles Calculations of the Electronic and Chemical Properties of Graphene, Graphane, and Graphene Oxide. *J. Mol. Model.* **2011**, *17*, 1133–1139.
- (39) Zhao, Y.; Schultz, N. E.; Truhlar, D. G. Design of Density Functionals by Combining the Method of Constraint Satisfaction with Parametrization for Thermochemistry, Thermochemical Kinetics, and Noncovalent Interactions. *J. Chem. Theory Comput.* **2006**, *2*, 364–382.
- (40) Frisch, M. J.; Trucks, G. W.; Schlegel, H. B.; Scuseria, G. E.; Robb, M. A.; Cheeseman, J. R.; Scalmani, G.; Barone, V.; Mennucci, B.; Petersson, G. A.; et al. *Gaussian 09*, revision A.02; Gaussian, Inc.: Wallingford, CT, 2009.
- (41) Silva, A. M.; Pires, M. S.; Freire, V. N.; Albuquerque, E. L.; Azevedo, D. L.; Caetano, E. W. S. Graphene Nanoflakes: Thermal Stability, Infrared Signatures, and Potential Applications in the Field of Spintronics and Optical Nanodevices. *J. Phys. Chem. C* **2010**, *114*, 17472–17485.